Correlation of Measured Soft X-Ray Pulses With Modeled Dynamics of the Plasma Focus

Sing Lee, S. H. Saw, Rajdeep Singh Rawat, Paul Lee, Alireza Talebitaher, Ali E. Abdou, Perk Lin Chong, Federico A. Roy, Jr, *Member, IEEE*, Arwinder Singh, D. Wong, and K. Devi

***Abstract*—The six-phase Lee model code is used to fit the computed current waveform to the measured current waveform of INTI plasma focus (PF; 2.2 kJ at 12 kV), a T2 PF device, operated as a source of neon soft X-ray (SXR) with optimum yield around 2 torr of neon. The characteristic He-like and H-like neon line SXR pulse is measured using a pair of SXR detectors with selected filters that, by subtraction, has a photon energy window of 900 to 1550 eV covering the region of the characteristic neon SXR lines. From the analysis of the fitted current and the measured SXR pulses, the characteristic neon SXR pulses are correlated to the pinch dynamics, and the subsequent slightly harder SXR pulses are correlated to the anomalous resistance phase. The characteristic neon SXR yield is measured; the pulse has a duration of 25 ns. The characteristic neon SXR typically starts 10 ns before the pinch phase and continues through the end of the 10-ns pinch phase, tailing into the anomalous resistance phase. Harder SXR pulses, probably Bremsstrahlung, are correlated to the anomalous resistance phase, with the main pulse occurring nearly 200 ns after the characteristic neon SXR pulse.**

***Index Terms*—Neon soft X-rays (SXR), plasma focus (PF) dynamics, PF modeling, SXR measurements.**

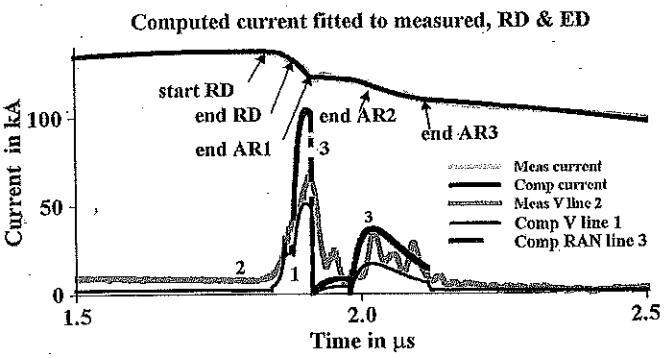

Fig. 1. Fitting computed current waveform to measured current waveform for the KSU PF. The time scale is expanded in this figure and shows the radial phases only [12]. The standard five-phase code provides a fit of the computed to the measured current waveform only up to the point "end RD." Beyond that point, fitting of the computed to the measured current waveform requires the extension to a six-phase code with the use of three anomalous resistances (RAN1, RAN2, and RAN3 labeled as "Computed RAN line 3") for the regions AR1, AR2, and AR3. Typically, the fitting is so good that the computed and measured current traces overlap and appear as one trace (the top trace).

I. Introduction

THE DYNAMICS of the plasma focus (PF) computed from the Lee model code [1] is found to be in general agreement with experimental measurements when the computed current waveform is properly fitted to the measured current waveform [1]–[11]. The features in agreement include the temporal profiles of the axial and the radial speeds.

Recently, it has been found [12] that, for modeling purposes, PF devices may be conveniently classified into T1 and T2, the former having low static inductance L_0 typically in tens of nanohenry while the latter typically having L_0 of more than 100 nH.

The T1 PF devices have measured current waveforms which are well fitted to the computed current waveforms using the standard five-phase model code, whereas T2 devices have a small computed current "regular" dip (RD) which could only be fitted to the first part of the measured current dip. The measured current dip then continues beyond the computed dip (RD) into a longer and deeper extended dip (ED) which cannot be fitted using the five-phase model code. The INTI PF is a typical T2-type PF device. To complete the fit for T2 devices, the five-phase Lee Model code was extended to the six-phase code with the addition of a postpinch phase of anomalous resistances. With this new six-phase code, the computed current waveform is fitted very well to the measured current waveform (see Fig. 1).

A question then arises: What is the correlation between the time history of the measured soft X-ray (SXR) pulse with the different phases of the computed current waveform which has been fitted to the measured current waveform? To answer this question entails the fitting of the current waveform in the region of the RD to an accuracy of 4 ns or better since the phase of greatest interest, the pinch phase, has a computed duration of around 10 ns for the INTI PF [3]. This is to ensure that we get the time position of the SXR pulse relative to the pinch phase with a time resolution of 40% of the pinch phase duration.

Manuscript received May 1, 2011; revised June 9, 2011; accepted August 19, 2011. Date of publication September 26, 2011; date of current version November 9, 2011.

S. Lee and S. H. Saw are with INTI International University, Nilai 71800, Malaysia, and also with the Institute for Plasma Focus Studies, Chadstone, Vic. 3148, Australia (e-mail: leesing@optusnet.com.au; sorheoh.saw@newinti.edu.my).

R. S. Rawat, P. Lee, and A. Talebitaher are with the National Institute of Education, Nanyang Technological University, Singapore 637616 (e-mail: rajdeep.rawat@nie.edu.sg; paul.lee@nie.edu.sg; mtalebi69@yahoo.com).

A. E. Abdou is with Kansas State University, Manhattan, KS 66506 USA (e-mail: aeabdou@ksu.edu).

P. L. Chong, F. A. Roy Jr., A. Singh, D. Wong, and K. Devi are with INTI International University, Nilai 71800, Malaysia (e-mail: perklin.chong@newinti.edu.my; federico.royjr@newinti.edu.my; arwinders.jigiris@newinti.edu.my; davidwm.wong@newinti.edu.my; kavurik.adevi@newinti.edu.my).

Color versions of one or more of the figures in this paper are available online at http://ieeexplore.ieee.org.

Digital Object Identifier 10.1109/TPS.2011.2166812

For several applications, we also need to differentiate the neon SXR into the characteristic He-like and H-like neon line radiation and the slightly harder SXR such as Bremsstrahlung emitted by hotter fully ionized neon plasmas. The characteristic radiation of the He-like and H-like neon consists of two dominant lines at 921 eV (13.447 Å) and 1020 eV (12.132 Å), contributing 80% of the characteristic neon SXR radiation. The remaining 20% comprises mixed lines and continuum radiation between 1070 and 1548 eV (8 and 11.568 Å) [13]. Since these characteristic He-like and H-like radiations are predominantly line radiations, we shall apply the term characteristic He-like and H-like neon line radiation to the sum of these emissions in the photonic energy window of 900–1550 eV (8–13.5 Å). Differentiating the neon SXR into characteristic neon line emission and the harder continuum SXR and correlating these separately to the various phases of the focusing plasmas provide useful information on applications and on the modeling.

II. Method

A. Experiment

We develop a method to reduce the electrical noise in the measured current waveform. A seven-turn Rogowski coil is used to record the rate of change of current dI/dt with the coil output connected to a digital storage oscilloscope (DSO) at a sample rate of 1 GSa/s at a frequency response of 200 MHz. The signal is then numerically integrated [14]. This method is found to give a signal with good frequency response and also reasonably free of electrical noise in the form of coil self-oscillations.

The SXR pulses [from two detector channels of diode X-ray spectrometer (DXS)] and the corresponding measured current and voltage are taken together on a four-channel DSO. The voltage signal was obtained using a resistive divider. This divider had been tested and showed a time response of 15 ns in the region [15].

The absorption filter method based on foil absorbers and silicon PIN diode detectors is used in the SXR spectrometer [16]. The two SXR detectors of the DXS are used together as a differentially filtered pair (Ch1 and Ch2 of DXS) to measure the characteristic He-like and H-like neon line SXR by the method of subtraction [17]. Each detector consists of a reverse-biased BXP65 PIN photodiode with a wide spectral range. The glass window of the BPX65 detector is removed, extending the spectral range and making the detector sensitive to SXR.

The foil filter of the first channel (Ch1) is designed so that Ch1 has the same sensitivity as the differently foil-filtered Ch2 over all wavelength range except in a window corresponding to the characteristic He-like and H-like neon line emission [16].

The characteristic He-like and H-like neon line emission and small amounts of continuum had been measured as [13]

921 eV: (13.447 Å)	65%	region 1 (strong line)
1020 eV: (12.132 Å)	15%	region 2 (strong line)
1548–1070 eV: (8–11.568 Å)	20%	region 3 (lines & continuum).

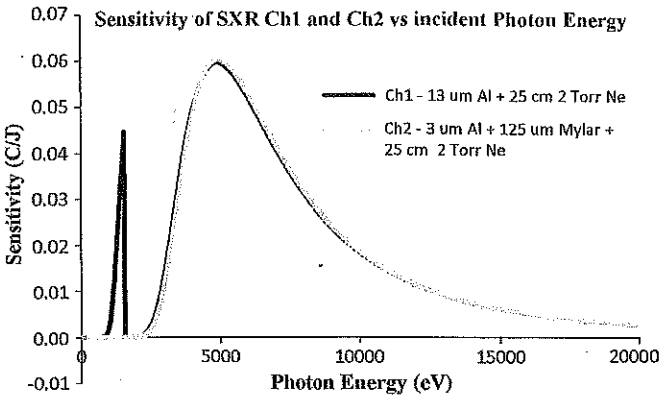

Fig. 2. Sensitivity of two channels. Ch1 and Ch2 are designed to have identical sensitivity curves for the region from around 1550 eV upward to 20 000 eV and beyond. The only difference in the two curves is that Ch1 has an additional region of sensitivity from 900 to 1550 eV (the spikelike feature between 0 and 2500 eV in the figure belongs to Ch1 only). In the other spectral (or photon energy) regions, there are two curves on top of each other, so the two curves are seen as one.

Therefore, the required window of sensitivity which Ch1 needs to have in addition to its otherwise identical sensitivity profile with Ch2 is the spectral or photonic energy range of 900–1550 eV. In designing the required filter, these emission wavelengths with expected line intensities are suitably weighted and factored in [18] to obtain the average sensitivity factor for the relatively narrow spectral window of 900–1550 eV.

A suitable pair is designed as follows. The first detector is covered with 13-μm Al (SXR Ch1), while the second detector is covered with 3 μm Al + 125 μm Mylar (SXR Ch2). Fig. 2 shows the sensitivities of each channel for this pair as a function of photon energy in electronvolts. The sensitivity of each channel is obtained using the quantum detection efficiency [19] of silicon, X-ray transmission efficiency through neon gas at different pressures and a fixed path length of 25 cm between the anode tip and the detector, and the X-ray attenuation length of solids [20]. The sensitivity curves are similar to the one shown in [17] as the filter materials are the same, although of slightly different thicknesses. At this point, we clarify that the filter pair that we are designing is not a Ross filter pair. A Ross filter pair [21] depends on absorption K-edges of two foil filters made from elements adjacent or nearly adjacent in the periodic table. In our case, the 125-μm Mylar filter (with 3-μm Al for blocking visible light) does not have an absorption edge in the range that we are using. So, the filter pair that we are using is not, strictly speaking, a Ross filter pair.

At the scale in Fig. 2, the two sensitivity curves are identical and appear as one overlapped curve from 0 to 20 000 eV, except for the sharp spike on the left side of the curve with a photonic energy range of 900–1550 eV. This spike (transmission window) belongs to Ch1 only.

The filter pair, for Ch1 and Ch2, is designed to give a difference window in the spectral region of the characteristic He-like and H-like SXR emission from neon 900–1550 eV [17]. Subtracting the signal of Ch2 from that of Ch1 thus allows the amount of characteristic neon SXR falling on the detectors to be computed. For example, if, for a shot, the difference signal

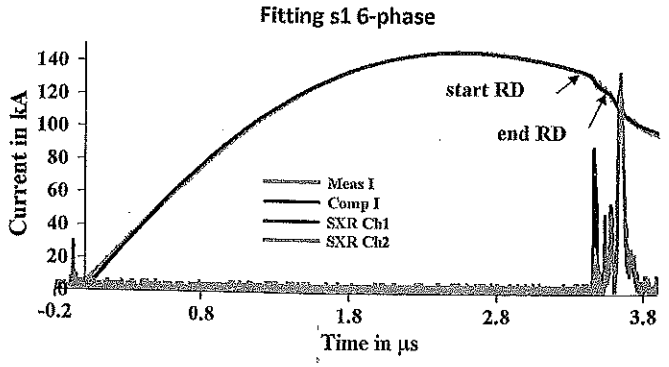

Fig. 3. Correlating currents and SXR channels. The computed current is fitted so well to the measured current that the two traces overlap, appearing as one trace (the top trace). SXR Ch1 and Ch2 also overlap very well except the first pulse (just after 3.4 μs), which is dominated by Ch1. The output of Ch1 is also slightly bigger than that of Ch2 for the second pulse, but the third pulse and very large fourth pulse (appearing just before 3.8 μs) have the outputs of Ch1 and Ch2 inseparably overlapping.

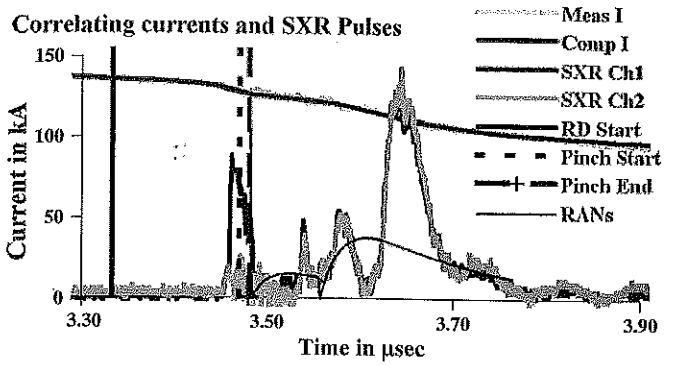

Fig. 4. This is an expansion of Fig. 3 from 3.3 to 3.9 μs. The top trace running across the figure is the overlapped lines of the computed and measured currents. The SXR Ch1 and Ch2 also overlap very well except the first pulse (just after 3.4 μs), which is dominated by Ch1. The three vertical lines are time markers for (from left) the start of radial phase or RD, and the start of pinch phase, which is also the end of RD.

between the two channels is zero, this means that no emission in the 900–1550-eV window is detected. This means that no characteristic neon SXR is detected. If there is a difference signal, it can only come from the 900–1550-eV window, and the difference signal is a measure of the characteristic neon SXR detected. If pulses are detected by the channels but there is no difference signal, that means that each channel is detecting a signal with photon energy considerably above 1550 eV. That means that, in that case, SXR harder than the characteristic neon SXR emission is detected.

Thus, capturing the SXR pulse on a DSO, the absolute amount of characteristic neon line SXR falling on the detector may be measured, and by assuming a point source radiating isotropically, the source yield can then be estimated by space integrating over 4π and time integrating over the duration of the pulse. Both detectors have been normalized to one another and are positioned side by side with the same distance to the focus position where the focus pinch emits the radiation to be detected.

In this manner, the experimentally measured current, tube voltage, and characteristic neon SXR yield are time correlated and ready for comparison with the time variations of computed current and trajectories. SXR harder than the characteristic neon SXR is also time correlated.

B. Numerical Experiment

The INTI PF had its electrical parameters determined as follows: $L_0 = 114$ nH, $C_0 = 30$ μF, and $r_0 = 13$ mΩ [22]; its tube parameters are $b = 3.2$ cm, $a = 0.95$ cm, and $z_0 = 16$ cm. The code is configured accordingly.

The computed current is fitted to the measured current [1]–[11] in steps described as follows.

First, the axial phase (see Fig. 3, where the axial phase is from $time = 0$ to the point indicated as "start RD") is fitted by varying f_m and f_c, and the three features of current rise slope, the topping profile, and the peak value of current are the fitting indicators. To compensate for the noninstantaneous switching of the spark gap as compared to the modeled instantaneous switching, a displacement in time is made to the computed current trace (relative to the measured trace). The critical topping region is expanded again and again as the fitting is fine tuned until an accuracy of 2–4 ns is typically achieved in the fitting of the computed to the measured current waveforms, particularly at the rollover region (or the start of the dip in the current trace) where the apparent beginning of the dip occurs. The end of the axial phase (indicated in Fig. 3 by the arrow "start RD") actually occurs a little before this rollover starts to become apparent.

Next, the radial phase (RD) is fitted by adjusting the radial parameters f_{mr} and f_{cr}. The features to observe for fitting most critically is the slope of the dip. The traces are expanded in the radial phase until the fit of the slopes is obtained with confidence at the 2–4-ns level. At these high levels of expansion, while the computed slope is being fitted, it may be necessary also to make further really fine tuning to the axial f_m to assist the fitting of the slope of the dip. The end result of this part of fitting is that the RD (from start to end) is fitted with sufficient accuracy to the first part of the measured current dip (the point "end RD" in Fig. 3).

Next, the computed current trace of the anomalous resistance regions [12] is fitted to the corresponding measured current trace one after the other. Typically, the anomalous resistance (RAN) region is divided into three regions, denoted as RAN1, RAN2, and RAN3.

We apply a resistance term to each of the three sections, the term being

$$R = R_0 \left[\exp(-t/t_2) - \exp(-t/t_1)\right].$$

We adjust the parameters R_0, t_2, and t_1 for each of the sections, as well as a fraction (*end fraction*) which terminates the term. Region RAN1 is fitted first; the parameters that are varied for the fitting are the amplitude R_0 of the anomalous resistance, the risetime t_1, and the falltime t_2, again expanding the traces until sufficient resolution is attained. When a satisfactory fit is obtained, then the next RAN2 region is fitted and so on for the RAN3 region.

As can be seen in Figs. 3 and 4, typically, the fit between the computed current trace to the measured one is so good that the two curves appear as one over almost the whole of the axial

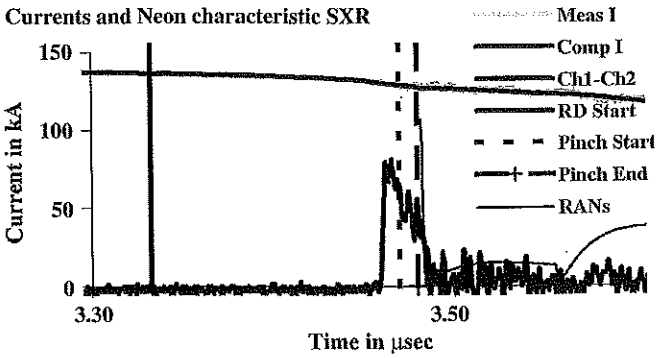

Fig. 5. This is derived from Fig. 4. The top trace running across the figure is the overlapped lines of the computed and measured currents. The pulse shown in this figure is the characteristic He-like and H-like neon SXR pulse obtained by subtracting Ch2 from Ch1 (see Fig. 4). The three RAN subphases are indicated by the thin line running across near the bottom.

phase and all the radial phases up to the end of the anomalous resistance phases.

C. Correlating the Time History

We had already determined that, at 12 kV, the INTI PF achieves optimum characteristic neon line SXR at a pressure of 2 torr. For the correlation work, we fired the INTI PF at this operation point and obtained a discharge current waveform together with the tube voltage, SXR Ch1 (filtered with 13-μm Al), and SXR Ch2 (filtered with 3-μm Al and 125-μm Mylar).

The measured SXR time profiles (two channels) are plotted from the digital data that are already time aligned to the measured time profile of current. The computed time profile of the current is fitted to the measured time profile of the current, described in Section II-B, thus time aligning the computed current profile to the measured current and, hence, to the SXR data. This computed current profile is computed in phases. Time markers (see Fig. 4) for the start of the radial RD phase, the start and end of the pinch phase, and the RAN1, RAN2, and RAN3 phases are placed on the comparative chart. In this way, the time periods of the characteristic neon SXR and the subsequent harder SXR pulses are correlated to the various radial phases of the focusing dynamics.

III. Results

Results are shown in Figs. 3–5 and discussed.

Fig. 3 shows that the computed current waveform is fitted very well to the measured current waveform, the two waveforms lying on top of each other, appearing as one up to the point $t = 3.9$ μs, which is the end of the RAN phases. Fig. 3 also shows the outputs of the two channels of SXR. The voltage waveform is not shown so as not to clutter Fig. 3. The four measured waveforms are displayed on the same four-channel DSO.

In Fig. 3, the start and end of the computed RD from the five-phase model are indicated by arrows. The anomalous resistance (RAN) regions lie past the end of the RD and extend to $t = 3.9$ μs, which is the end of the RAN region beyond which the fitting of computed and measured current waveforms is stopped.

Fig. 4 shows an expansion of Fig. 3 for the region 3.3–3.9 μs. It shows the outputs of the two SXR channels. From Fig. 4, we see that the first SXR pulse straddling the pinch duration is predominantly characteristic neon SXR (since there is a difference pulse). After the pinch phase, there is a short (few nanoseconds) RAN1 phase which coincides with the tail of the characteristic neon SXR pulse. The three RAN subphases are indicated by the thin "humpy" line running across near the bottom of Fig. 4. The first RAN subphase is of very short duration, shown by the almost vertically dropping thin line just after the end of the pinch phase (just resolved in the more highly expanded Fig. 5). Toward the end of the RAN2 phase, there is a sharp SXR pulse with a duration of less than 10 ns (see Fig. 4).

This pulse is harder SXR than the characteristic neon SXR lines, as is evidenced by the fact that the SXR Ch1 and Ch2 have almost identical outputs over the duration of this pulse, so that the difference of the two channels is practically zero. Then, at the start of RAN3, there is a similar SXR pulse of slightly higher amplitude but larger pulse duration of about 40 ns. The difference of the two channels over this pulse is also nearly zero, which indicates that the photon energy of this pulse is primarily harder than the characteristic neon SXR. Finally, between 3.6 and 3.7 μs, the main SXR pulse of this shot is emitted with a much larger amplitude (two times bigger) and a larger duration (more than 50 ns). This is the major SXR emission of this shot, and the emission is not characteristic neon SXR but is a harder SXR possibly from Bremsstrahlung coming from the fully ionized neon plasma of the type observed by others [23].

Fig. 5 is derived from Fig. 4 and shows the correlation of the measured (and computed) current with the characteristic He-like and H-like neon SXR which is the difference pulse obtained by subtracting SXR Ch2 from SXR Ch1 in Fig. 4. Also shown in Fig. 5 are time markers (vertical line) indicating from the computed results the start of the radial phase (solid vertical line) and the start and end of the focus pinch phases (dashed vertical lines). The RAN subphases are also indicated by the anomalous resistances (denoted by the light "humpy" line in arbitrary units).

The results show (for this particular shot) that the characteristic neon SXR starts strongly some 10 ns before the pinch phase (see Fig. 5); the pulse drops in amplitude through the 10-ns duration of the pinch phase and continues to drop to zero for another 5 ns after the pinch phase into the first anomalous resistive (RAN) phase. There is little or no characteristic neon SXR beyond this single pulse of SXR which lasts some 25 ns in total duration, straddling the 10-ns pinch phase. This characteristic He-like and H-like neon SXR pulse for this shot is integrated and found to have a radiation yield of 1.2 J.

Analysis of a number of shots at 12-kV 2-torr neon establishes that the correlation of Figs. 4 and 5 is typical of most of the shots. The characteristic neon SXR line yields of these typical shots at 12-kV 2-torr neon lie in the range of 1–2 J. There are also a lesser number of shots which give higher neon yields of 3–4 J. These are characterized by much wider pulses, some with significant contributions of characteristic neon SXR in the RAN regimes.

IV. Conclusion

The SXR pulses emitted from the INTI PF (one of the UNU ICTP PFF series) at 12-kV 2-torr neon (optimum characteristic neon line yield condition) are differentiated into characteristic He-like and H-like neon line SXR within the spectral window of 900–1550 eV and other (noncharacteristic) neon SXR emission with photonic energy higher than 1550 eV. These SXR emissions are carefully correlated to the time profiles of the measured and fitted computed currents. It is found typically that the characteristic He-like and H-like neon line SXR is emitted 10 ns before the pinch phase, achieving peak amplitude during these 10 ns, and then continues to be emitted with lower amplitude through the 10-ns pinch phase, then dropping to zero amplitude over another 5 ns as the plasma goes through its first anomalous resistance RAN1. During the second RAN period, there is a sharp (few-nanosecond duration) SXR pulse with only a very small amount of characteristic neon line SXR; the emission in this pulse is SXR harder than 1550 eV. During the third RAN period, there are two pulses of similar noncharacteristic neon SXR (harder than 1550 eV). The first of these has a duration of 40 ns occurring at the start of RAN3 subphase. The second of these is the main SXR pulse for this shot with a much higher amplitude and a duration of more than 50 ns.

These results may be further summarized as follows: The characteristic He-like and H-like neon line SXR pulse straddles the pinch phase, emitting strongly before, during, and a little after the pinch phase of the focusing action. After the pinch phase follows the anomalous resistance phase, during which several harder SXR pulses are emitted of primarily noncharacteristic neon SXR, possibly Bremsstrahlung.

These results have implications in improving the model code for the computation of characteristic He-like and H-like neon line SXR yield.

References

[1] S. Lee, Radiative Dense Plasma Focus Computation Package: RADPF, 2010. [Online]. Available: http://www.intimal.edu.my/school/fas/UFLF/File1RADPF.htm and http://www.plasmafocus.net/IPFS/modelpackage/File1RADPF.htm

[2] M. Akel, S. Al-Hawat, S. H. Saw, and S. Lee, "Numerical experiments on oxygen soft X-ray emissions from low energy plasma focus using Lee model," *J. Fusion Energy*, vol. 29, no. 3, pp. 223–231, 2010.

[3] S. H. Saw, P. C. K. Lee, R. S. Rawat, and S. Lee, "Optimizing UNU/ICTP PFF for neon operation," *IEEE Trans. Plasma Sci.*, vol. 37, no. 7, pp. 1276–1282, Jul. 2009.

[4] S. Lee, P. Lee, S. H. Saw, and R. S. Rawat, "Numerical experiments on plasma focus pinch current limitation," *Plasma Phys. Control. Fusion*, vol. 50, no. 6, p. 065012, Jun. 2008.

[5] S. Lee and S. H. Saw, "Pinch current limitation effect in plasma focus," *Appl. Phys. Lett.*, vol. 92, no. 2, p. 021503, Jan. 2008.

[6] S. Lee, "Neutron yield saturation in plasma focus—A fundamental cause," *Appl. Phys. Lett.*, vol. 95, no. 15, p. 151503, Oct. 2009.

[7] S. Lee, R. S. Rawat, P. Lee, and S. H. Saw, "Soft X-ray yield from NX2 plasma focus," *J. Appl. Phys.*, vol. 106, no. 2, p. 023309, Jul. 2009.

[8] S. Lee, S. H. Saw, P. C. K. Lee, R. S. Rawat, and H. Schmidt, "Computing plasma focus pinch current from total current measurement," *Appl. Phys. Lett.*, vol. 92, no. 11, p. 111501, Mar. 2008.

[9] S. Lee and S. H. Saw, "Neutron scaling laws from numerical experiments," *J. Fusion Energy*, vol. 27, no. 4, pp. 292–295, 2008.

[10] S. Lee, "Current and neutron scaling for megajoule plasma focus machines," *Plasma Phys. Control. Fusion*, vol. 50, no. 10, p. 105005, Oct. 2008.

[11] S. Lee, S. H. Saw, P. Lee, and R. S. Rawat, "Numerical experiments on plasma focus neon soft X-ray scaling," *Plasma Phys. Control. Fusion*, vol. 51, no. 10, p. 105 013 (8pp), Oct. 2009.

[12] S. Lee, S. H. Saw, A. E. Abdou, and H. Torreblanca, "Characterizing plasma focus devices—Role of the static inductance—Instability phase fitted by anomalous resistances," *J. Fusion Energy*, vol. 30, no. 4, pp. 277–282, Aug. 2011, DOI: 10.1007/s10894-010-9372-1.

[13] L. Mahe, "Soft X-rays from compact plasma focus," Ph.D. dissertation, Nanyang Technol. Univ., Singapore, 1996.

[14] S. Lee, S. H. Saw, R. S. Rawat, P. Lee, R. Verma, A. Talebitaher, S. M. Hassan, A. E. Abdou, M. Ismail, A. Mohamed, H. Torreblanca, S. Al Hawat, M. Akel, P. L. Chong, F. Roy, A. Singh, D. Wong, and K. Devi, "Measurement and processing of fast pulsed discharge current in plasma focus machines," *J. Fusion Energy*, Jul. 27, 2011, DOI: 10.1007/s10894-011-9456-6, to be published.

[15] S. Lee, T. Y. Tou, S. P. Moo, M. A. Eissa, A. V. Gholap, K. H. Kwek, S. Mulyodrono, A. J. Smith, Suryadi, W. Usada, and M. Zakaullah, "A simple facility for the teaching of plasma dynamics and plasma nuclear fusion," *Amer. J.*, vol. 56, no. 1, pp. 62–68, 1988.

[16] W. Wang, A. Patran, S. Lee, and P. Lee, "Simple, effective multichannel pin diode X-ray spectrometer system," *Sing. J. Phys.*, vol. 17, no. 1, p. 27, 2001.

[17] D. Wong, A. Patran, T. L. Tan, R. S. Rawat, and P. Lee, "Soft X-ray optimization studies on a dense plasma focus device operated in neon and argon in repetitive mode," *IEEE Trans. Plasma Sci.*, vol. 32, no. 6, pp. 2227–2235, Dec. 2004.

[18] Z. Guixin, "Plasma soft X-ray source for microelectronic lithography," Ph.D. dissertation, Nanyang Technol. Univ., Singapore, 1999.

[19] A. G. Michette and C. J. Buckley, *X-Ray Science and Technology*. Bristol, U.K.: Inst. Phys. Publishing, 1993, p. 249.

[20] B. L. Henke, E. M. Gullikson, and J. C. Davis, "X-ray interactions: Photoabsorption, scattering, transmission, and reflection at $E = 50$–$30,000$ eV, $Z = 1$–92," *At. Data Nucl. Data Tables*, vol. 54, no. 2, pp. 181–342, Jul. 1993.

[21] E. Kroupp, A. Starobinets, E. Kłodzh, Y. V. Ralchenko, Y. Maron, I. N. Bogatu, and A. Fisher, "Investigation of Ne IX and Ne X line emission from dense plasma using Ross-filter systems," *J. Appl. Phys.*, vol. 92, no. 9, pp. 4947–4951, Nov. 2002.

[22] S. H. Saw, S. Lee, F. Roy, P. L. Chong, V. Vengadeswaran, A. S. M. Sidik, Y. W. Leong, and A. Singh, "*In situ* determination of the static inductance and resistance of a plasma focus capacitor bank," *Rev. Sci. Instrum.*, vol. 81, no. 5, p. 053505, May 2010.

[23] A. Bernard, H. Bruzzone, P. Choi, H. Chuaqui, V. Gribkov, J. Herrera, K. Hirano, A. Krej, S. Lee, C. Luo, F. Mezzetti, M. Sadowski, H. Schmidt, K. Ware, C. S. Wong, and V. Zoita, "Scientific status of plasma focus research," *J. Moscow Phys. Soc.*, vol. 8, pp. 93–170, 1998.

Sing Lee received the B.Sc. and M.Sc. degrees from the University of Malaya (UM), Kuala Lumpur, Malaysia, in 1964 and 1966, respectively, and the Ph.D. degree from the Australian National University, Canberra, Australia, in 1970.

He was a Professor of applied physics and headed research groups in plasma and pulse technology and the Physics Department, UM, and was the Head of the Division of Physics and the Head Academic Group of Natural Sciences, National Institute of Education, Nanyang Technological University, Singapore, Singapore. He was an Alexander von Humboldt Fellow at Kernforschunglange, Juelich, Germany, from 1975 to 1976, a Commonwealth Academic Staff Fellow at Imperial College London, London, U.K., from 1981 to 1982, and a Visiting Professor and a United Nations University Special Fellow at Flinders University, Adelaide, Australia, from 1986 to 1987. He is currently an Adjunct Professor (honorary) of INTI International University, Nilai, Malaysia. He is currently the Founding Director of the (Web-based) Institute for Plasma Focus Studies, Chadstone, Australia.

Prof. Lee was the Founder President of Asian African Association for Plasma Training (AAAPT); the Associate Director of the AAAPT Research and Training Centre, Institute of Physics, Academia Sinica, Beijing, China; a Far Eastern Representative of the International Centre for Theoretical Physics; and an ardent advocate and an implementor of south–south technology creation and transfer, in plasma fusion, laser, and pulse technology. He is also a Chartered Physicist and a Fellow of the Institute of Physics (U.K.), a life and Honorary Fellow of the Institute of Physics Malaysia, a Life Fellow of Singapore Institute of Physics and the Samahang Pisika ng Pilipinas, and an honorable member of the Turkish Science and Research Foundation TUBAV.

S. H. Saw received the B.Sc.(Hons.) and Ph.D. degrees in physics from the University of Malaya, Kuala Lumpur, Malaysia, in 1985 and 1991, respectively, and the M.A. degree in educational management from The University of Nottingham, Nottingham, U.K., in 1997.

She is currently a Professor and the Pro Vice-Chancellor for Education Quality and Innovation at INTI International University, Nilai, Malaysia, where she is the Director of the Centre for Plasma Research. She is the Codirector of the Institute for Plasma Focus Studies, Chadstone, Australia, and the designated delegate of INTI IU for the Asian African Association for Plasma Training. Her current research interests include plasma physics and innovation in education.

Prof. Saw was conferred an honorary membership of the Turkish Science and Research Foundation TUBAV in 2009.

Rajdeep Singh Rawat was born in Delhi, India, on September 5, 1965. He received the B.Sc.(Hons.) degree in physics, the M.Sc. degree in physics, and the Ph.D. degree from University of Delhi, Delhi, India, in 1985, 1987, and 1994, respectively.

He lectured at the Department of Physics and Electronics, SGTB Khalsa College, University of Delhi, from 1992 to 2000. He was instrumental in setting up the Plasma Focus Laboratory, University of Delhi, with support from ICTP-UNU Pulse Plasma Program of the Asian African Association for Plasma Technology (AAAPT) and pioneered the technique of material processing and thin-film deposition using single-shot plasma focus device. In December 2000, he joined the National Institute of Education, Nanyang Technological University, Singapore, Singapore, as an Assistant Professor, where he has been an Associate Professor since October 2005. He has authored more than 110 research papers in international journals and edited two conference proceedings. His research work includes material processing and thin-film deposition using focus device and basic studies on dense plasma focus device using laser shadowgraphy, diode X-ray spectrometer, and Faraday cup. His current research interests include deposition of magnetic nanophase thin films and magnetic nanoparticles using focus device and pulsed high-power lasers, diluted magnetic semiconductor thin films of transition metal-doped ZnO, development of low-energy miniature plasma focus device as a repetitive neutron source at 10 Hz, and development of 20-kJ medium-energy plasma focus device at NIE for investigation on the effect of high flux neutrons on materials.

Prof. Rawat is currently the Secretary for AAAPT and a Fellow and a council member of the Institute of Physics Singapore.

Paul Lee received the B.Sc.(Hons.) and Ph.D. degrees from the University of London (Imperial College), London, U.K., in 1992 and 1996, respectively, and the PGDipTHE degree from Nanyang Technological University, Singapore, in 1999.

He was a Visiting Associate Professor at the University of Washington, Seattle, and the Technological Educational Institute of Crete, Heraklion, Greece, during 2007. He is currently an Associate Professor with the National Institute of Education, Nanyang Technological University. His current research interests include plasma physics, materials science, and physics education.

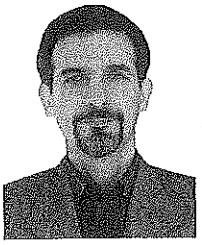

Alireza Talebitaher received the B.Sc. degree in electrical/electronic engineering from Amirkabir University of Technology (formerly named Tehran Polytechnic), Tehran, Iran, in 1994. Since 2008, he has been working toward the Ph.D. degree in experimental plasma physics in the National Institute of Education (NIE), Nanyang Technological University, Singapore, Singapore.

From 1994 until 2008, he was with Van de Graaff Laboratory, Fusion Research Center, and Plasma Physics Research Center, Tehran, as a Staff Engineer and an Electronics Laboratory Instructor. His current research is focused on using the coded aperture imaging technique for the investigation of spatial distribution of fusion source in plasma focus devices.

Dr. Talebitaher is a member of the Institute of Physics Singapore.

Ali E. Abdou received the B.S. degree in nuclear engineering from Alexandria University, Alexandria, Egypt, in 1992 and the M.S. degree in nuclear engineering, the M.S. degree in computational sciences, and the Ph.D. degree in nuclear engineering from the University of Wisconsin, Madison, in 2002, 2003, and 2005, respectively.

He has over 15 years of experience in the nuclear science and engineering fields. From 1994 to 1999, he participated in the design, preoperation, inauguration, and operation of Egypt's second test and research nuclear reactor ETRR-2. From 2005 to 2009, he was a Senior Process Development Engineer with Portland Technology Development, Intel Corporation, where he worked in the area of plasma etching and semiconductor nanofabrication. He was responsible for the process development of shallow trench isolation for 65-, 45-, and 32-nm nodes. He has wide expertise in plasma processing techniques used in the fabrication and characterization of semiconductor nano-/microstructures. In early 2009, he joined the Department of Mechanical and Nuclear Engineering, Kansas State University, Manhattan, as an Assistant Professor of nuclear engineering. He has authored or coauthored over 48 research publications. His current research interests include the development of nanosecond compact multiradiation sources based on the dense plasma focus, the research and development of plasma etching in semiconductor nanofabrication, optical emission spectroscopy, and X-ray emission from plasmas.

Dr. Abdou is a licensed radiation protection and health physicist from Argentinean ENRN and Egyptian NRC, which he received in 1996 and 1997, respectively.

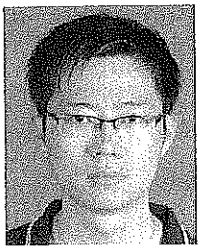

Perk Lin Chong received the B.Eng. degree from the University of Liverpool, Liverpool, U.K., in 2000 and the Ph.D. degree from The University of Birmingham, Birmingham, U.K., in 2006.

He is currently a Senior Lecturer with INTI International University, Nilai, Malaysia, where he is a Reviewer of *INTI Journal*. His research attention is on numerical computation of plasma focus.

Dr. Chong is a member of The Institution of Engineers Malaysia. He is active in a number of research activities: He was the Cochair of the Seminar on Plasma Focus Experiments (SPFE 2010), Secretariat of SPFE 2011, and the Technical Chair of the International Conference on Recent and Emerging Advanced Technologies in Engineering (in 2009), and he was in the Technical Committee (Mechanical Division) of the International Conference on CAD/CAM, Robotics and Factories of the Future (CARs&FOF 2011).

Federico A. Roy, Jr. (M'09) received the B.Sc. degree in electrical engineering from FEATI University, Manila, Philippines, in 1982 and the M.S. degree in electrical engineering from Universiti Tenaga Nasional, Putrajaya, Malaysia, in 2004. He is currently working toward the Ph.D. degree in applied physics at INTI International University, Nilai, Malaysia.

He is currently a Senior Lecturer with the Faculty of Engineering and Information Technology (FOEIT), INTI International University. His research areas include soft X-ray (plasma focus machine), power systems, and teaching and learning.

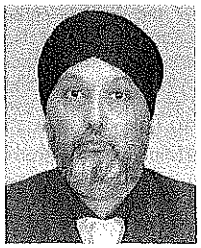

Arwinder Singh received the B.Eng. degree in electrical and electronic engineering from the University of Aberdeen, Aberdeen, U.K., in 1993, the M.Sc. degree in information technology from Universiti Putra Malaysia, Serdang, Malaysia, in 2002, and the M.Eng. degree in telecommunication from Multimedia University, Cyberjaya, Malaysia, in 2006.

He is currently teaching at INTI International University, Nilai, Malaysia. His current research is focused on the comparative study on plasma focus machines.

D. Wong, photograph and biography not available at the time of publication.

K. Devi, photograph and biography not available at the time of publication.